Available online at www.sciencedirect.com
SCIENCE DIRECT®
Journal of Solid State Chemistry 178 (2005) 2383–2389
JOURNAL OF SOLID STATE CHEMISTRY
www.elsevier.com/locate/jssc

Needle-like calcium carbonate assisted self-assembly of mesostructured hollow silica nanotubes

Jie-Xin Wang[a], Li-Xiong Wen[a,*], Run-Jing Liu[b], Jian-Feng Chen[a,b,*]

[a]Key Lab for Nanomaterials, Ministry of Education, Beijing University of Chemical Technology, Beijing 100029, PR China
[b]Research Center of the Ministry of Education for High Gravity Engineering and Technology, Beijing University of Chemical Technology, Beijing 100029, PR China

Received 26 March 2005; received in revised form 16 May 2005; accepted 22 May 2005

Abstract

Mesostructured hollow silica nanotubes (MHSNTs) were successfully produced via the self-assembly of C_{16}TMABr and silica species on the surface of needle-like calcium carbonate nanoparticles in an alkaline medium at room temperature. The characterization of MHSNTs by transmission electron microscopy (TEM), scanning electron microscopy (SEM), pore size distribution (PSD) and Brunauer–Emmett–Teller (BET) indicated that MHSNTs had uniform tubular hollow structures with big openings, a length of 1.5–2.0 μm, an inner diameter of 150–200 nm at the open end and 50–60 nm at the closed end, and a wall thickness of 20–30 nm, as well as a narrow PSD around 2.3 nm in the shells and a BET surface area as high as ~975.3 m^2/g. By small-angle X-ray diffraction (XRD), BET and pore structure analysis, it was found that more uniformly structured mesopores could be formed by the method of removing the double templates simultaneously through a solvent extraction process, as compared to the separate removal of the double templates by calcinating and then etching in an acidic solution, and the amount of C_{16}TMABr affected the mesoporous structures of MHSNTs greatly. The formation processes of MHSNTs were also studied with XRD and FTIR.

Keywords: Mesostructure; Hollow silica nanotubes; Double templates; Self-assembly; Solvent extraction

1. Introduction

Recently, much attention has been given to the development of novel porous materials with various dimensions. Among them, the fabrication of one-dimensional nanostructures has attracted a great deal of interest owing to their fascinating geometries, physical properties, and numerous potential applications [1–3]. In particular, hollow silica nanotubes are biocompatible, photoluminescent, and their surfaces are accessible and can be modified [4–6]. Therefore, they can be applied to the areas of drug delivery, adsorption, catalysis, bioseparation, and the protection of environmentally sensitive species [7–9]. To date, most fabrication methods for hollow silica nanotubes have focused on the use of various templates, such as biological substrates, surfactants, carbon nanotubes, vertical silicon nanowires, gold nanorods, reverse microemulsion, etc. [10–21]. Such template synthesis can produce tubular structures with uniform diameters and lengths. However, this template-directed technique is not suitable for large-scale fabrication of silica nanotubes, because the entire procedure is complicated or the template is expensive. Furthermore, the channels on the shell of most porous hollow silica tubes often appeared as disordered micropores, and hence limiting

*Corresponding authors. Key Lab for Nanomaterials, Ministry of Education, Beijing University of Chemical Technology, Beijing 100029, PR China. Fax: +86 10 64434784.
E-mail addresses: wenlx@mail.buct.edu.cn (L.-X. Wen), chenjf@mail.buct.edu.cn (J.-F. Chen).

0022-4596/$ - see front matter © 2005 Published by Elsevier Inc.
doi:10.1016/j.jssc.2005.05.025

their applications. Therefore, synthesis of hollow tubes with hierarchal morphologies is crucial for their properties and applications.

In this paper, we present a facile process to prepare mesostructured hollow silica nanotubes (MHSNTs) with mesopores in the wall, based on our previous work about the synthesis of hollow silica spheres with mesoporous shells [22], by using inexpensive needle-like $CaCO_3$ as the tube templates and C_{16}TMABr as the mesostructured channel directing agent. In our previous studies [23,24], the pores on the shells of silica nanotubes were usually disordered micropores, which limited their applications. Therefore, the preparation of MHSNTs will improve the pore structures of the hollow tube materials, and hence increasing their potential application scopes significantly. Our aim in this paper is to explore the formation processes of MHSNTs, and to study the effects of C_{16}TMABr and different methods for removing the templates on the structures of MHSNTs.

2. Experimental

In this work, needle-like $CaCO_3$ nanoparticles as tube templates consisted mainly of aragonite phase with a little calcite content and were synthesized in a high-gravity environment generated by a rotating packed bed reactor [25]. Other chemicals used in the experiments were obtained from commercial sources as analytical reagents and used without further purification. Deionized water was used throughout the study.

The preparation of MHSNTs was achieved with a similar but modified technology as reported in our previous work [22,24]. In a typical synthesis, needle-like $CaCO_3$ particles were firstly dispersed in a mixed solution of ethanol and deionized water under sonication. C_{16}TMABr and aqueous ammonia (25 wt%) were then added into the suspension in sequence under vigorous stirring. After being stirred for 1 h, tetraethoxysilane was added into the mixture dropwise. The added amount of each material was controlled to have the molar composition of the resulting synthesis gels as $1SiO_2$: $1.4CaCO_3$: xC_{16}TMABr: $11NH_3H_2O$: 58EtOH: $144H_2O$, where $x = 0$ for ratio D, 0.139 for ratio C, 0.185 for ratio B, and 0.278 for ratio A. The mixture was further stirred for another 4 h at room temperature, and the produced white precipitate was then collected by filtration and washed with a large amount of deionized water and ethanol to remove the extra ammonia and surfactant absorbed on the surface of the composite, which was designated as pre-calcinated powders. After the pre-calcinated powders were dried overnight at 363 K, heated to 823 K in air at a rate of 1 K/min, they were calcinated at 823 K for 5 h. Finally, the as-prepared composite solids were put into a dilute acetic acid solution for 12 h to remove the $CaCO_3$ templates. The resulting gel was filtered and rinsed again, followed by drying in a vacuum oven at 373 K for 10 h to obtain the MHSNTs. The above procedure for the removal of the templates was designated as Method I.

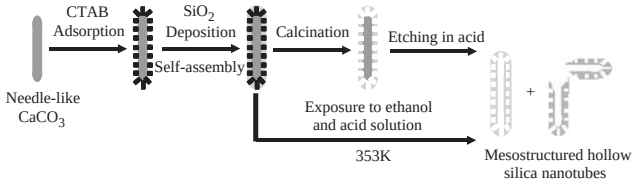

Fig. 1. The overall procedure for synthesizing mesostructured hollow silica nanotubes.

For comparison, a different method to remove the double templates was carried out as follows. The above-prepared pre-calcinated powders were added in an acidic organic solvent containing 300 mL of ethanol and 40 mL of acetic acid (or 5 mL of HCl solution) at 353 K and kept under stirring for 12 h. Such a process could simultaneously remove C_{16}TMABr by the solvent extraction and $CaCO_3$ by reacting with the acidic solutions. The mixture was then filtered, rinsed and dried to obtain the MHSNTs. These processes for removing the templates were named Method II (acetic acid) and Method III (HCl), respectively.

The overall procedures for synthesizing MHSNTs are illustrated in Fig. 1. The morphology and structures of the prepared samples were characterized by transmission electron microscopy (TEM, HITACHI, H-800 and FE-TEM, JEOL JEM-2010F) and scanning electron microscopy (SEM, JEOL, JSM-6301F). The elemental analysis of the samples was performed by an energy dispersive spectroscope (EDS, LINK, ISIS-300). X-ray diffraction (XRD) patterns were recorded on a diffractometer (Rigaku, D/Max2500VB2+/PC) with Cu$K\alpha$ radiation of wavelength 0.154056 nm. The nitrogen adsorption–desorption isotherms were measured on an ASAP 2010 surface area analyzer (Micromeritics), in which the samples were outgassed first in vacuum at 473 K overnight and the measurements were then carried out at 77 K. The pore size distribution (PSD) was determined by the Barret–Joyner–Halenda (BJH) method and the surface area was calculated by the Brunauer–Emmett–Teller (BET) method. The samples were also analyzed with an infrared spectrometer (IR, BRUKER, VECTOR-22).

3. Results and discussion

In the procedures for synthesizing MHSNTs, needle-like calcium carbonate nanoparticles, which usually carry negative charges in a basic solution (pH > 8), were used to assist the self-assembly of inorganic silica and

the surfactant micelles under an alkaline condition at room temperature. Positively charged surfactant micelles were absorbed on the surface of $CaCO_3$ particles because of the electrostatic interaction. Silicate species and the surfactant micelles may be self-assembled into a two-dimensional (2D) hexagonal arrangement on the surface of calcium carbonate particles, similar to the formation process on the surface of PS beads mentioned in the literature [26]. Upon calcination at high temperature and etching in an acidic solution, or exposure to a mixed solution of ethanol and acid, the surfactant molecules and the $CaCO_3$ particles were removed in sequence or simultaneously, leading to the formation of MHSNTs. The surfactant directed the silica into mesoporous 2D hexagonal arrangement while the needle-like $CaCO_3$ particles organized the silica material into hollow tube shape. Upon thermal treatment or solvent extraction to remove the surfactant templates, mesopores were created on the wall of the hollow silica nanotubes and the pore size fell into a 2–3 nm region.

The TEM image of the needle-like $CaCO_3$ templates, SEM, TEM images and EDS spectrum of the MHSNTs samples are given in Fig. 2. SEM and TEM images of MHSNTs demonstrated that the as-prepared MHSNTs had almost the same morphology as the previously fabricated hollow silica tubes reported in our recent publications [23,24]. As shown in Fig. 2, MHSNTs had an empty inner core with the similar shape as the $CaCO_3$ templates, which indicated that needle-like $CaCO_3$ particles functioned as the structure-directing agents in the synthesis, and the average inner diameters at the open ends and the closed ends of MHSNTs were 150–200 and 50–60 nm, respectively, which are close to the average diameters of the $CaCO_3$ templates near the middle and at the ends. The walls of the hollow tubes had a thickness of 20–30 nm, which could be controlled by the $SiO_2/CaCO_3$ ratio in the preparation. However, in many cases, the length of MHSNTs (1.5–2.0 μm) was approximately half of the $CaCO_3$ template length, owing to the breakage of the $CaCO_3/SiO_2$ composite or the hollow particles during the preparation process. It was also this breakage that resulted in the formation of the openings of the prepared MHSNTs. The existence of this big opening would allow the large internal void space of the tube to be more accessible to larger entities such as viruses or macromolecules, which will be practically appreciated in many applications such as bio-immobilization. The strong contrast between the dark edge and the pale center in Fig. 2(c and d) was evidence for the hollow nature of the nanotubes [27], which was also confirmed by the openings in Fig. 2(b). Fig. 2(e) revealed the presence of Si and O and the absence of Ca in the MHSNTs with carbon introduced by the carbon film on the TEM grid, indicating the complete removal of the $CaCO_3$ templates.

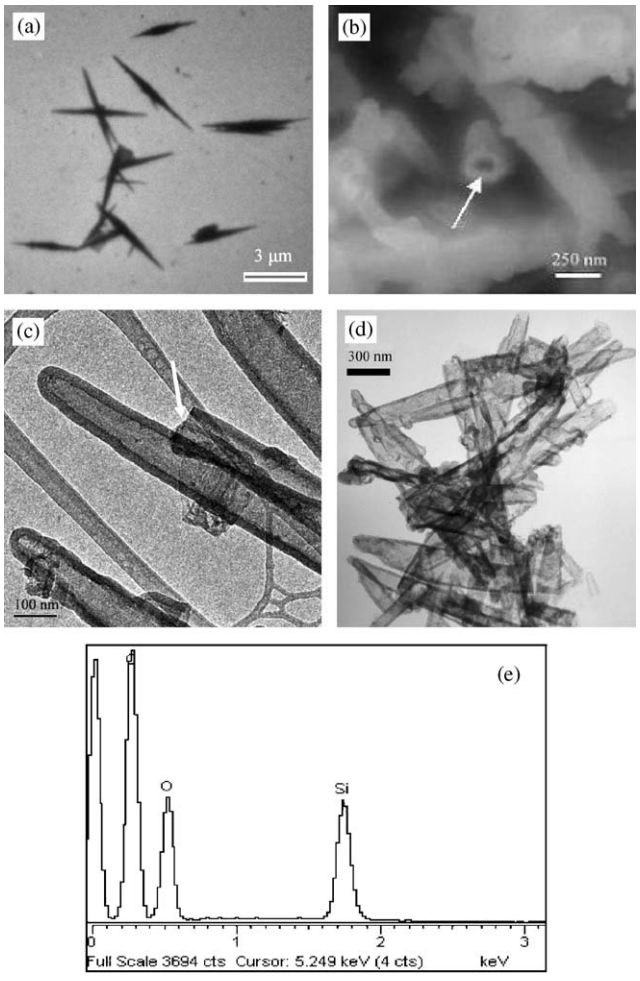

Fig. 2. TEM image for needle-like $CaCO_3$ nanoparticles (a); SEM (b), TEM (c,d) images and EDS (e) analysis of MHSNTs.

Unlike the previously prepared hollow silica nanotubes with disordered micropores [23,24], the as-synthesized MHSNTs had uniform mesostructure of nanochannels on the shell and at the openings. The samples were subjected to FE-TEM analysis. Fig. 3(a) and 3(b) showed part of the nanotubes and demonstrated the hollow core of the MHSNTs again. Though nanochannels on the shell could only be observed roughly from Fig. 3(a) and (b), their existence was clearly illustrated in Fig. 3(c) and (d). Fig. 3(c) exhibited the pore structure of a small region on the external surface of the MHSNTs. The tiny disks of light contrast correspond to the pores, while the dark networks represent the silica walls. Most of the pores are worm-like mesopores and lack a long-range order, which is in agreement with the following XRD pattern that possesses only one peak in a small-angle range. A TEM micrograph at the opening of the MHSNTs was illustrated in Fig. 3(d). It enabled the interesting nanochannels on the shell to be examined and clearly showed some order-arrayed stripe nanochannels, which

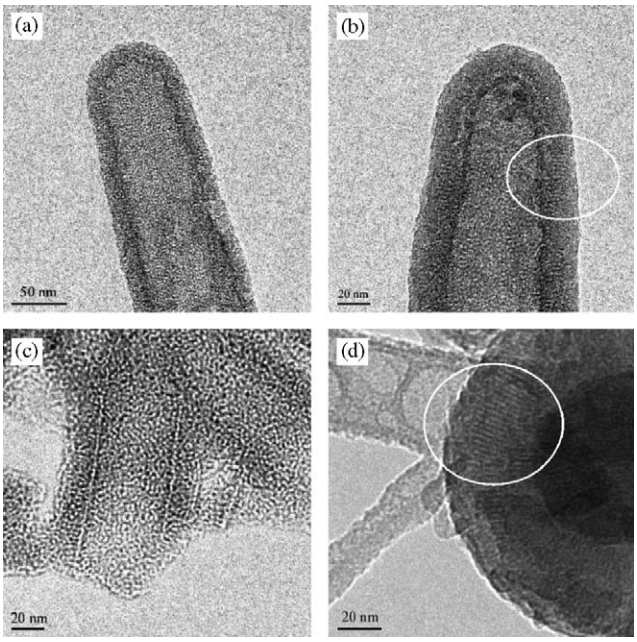

Fig. 3. FE-TEM images of MHSNTs.

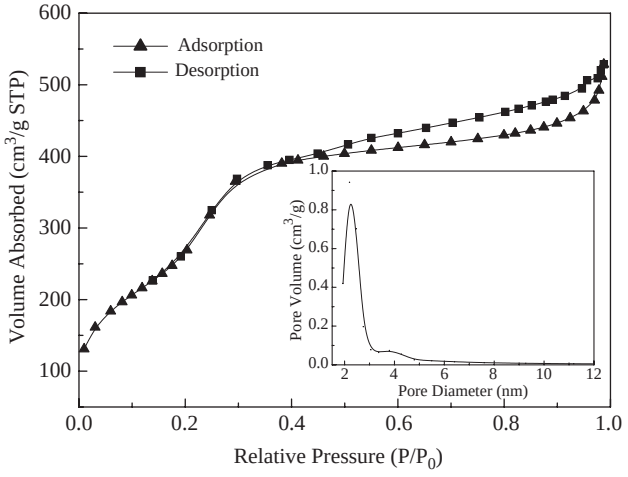

Fig. 4. N_2 adsorption and desorption isotherms for MHSNTs by Methods I–III and the corresponding BJH pore size distribution calculated from the desorption branch of the isotherms (insert).

are nearly perpendicular to the shell, with a diameter of about 2–3 nm. Different from those big openings, the worm-like mesopores and some order-arrayed stripe nanochannels on the shells would allow a simultaneous embedding of smaller molecules.

The typical N_2 adsorption–desorption isotherms and BJH PSDs were illustrated in Fig. 4. They were typical type IV isotherms and displayed a little hysteresis loop, indicating that the pores may not be very well ordered. A clear adsorption step occurred at a relative pressure between 0.15 and 0.3, which is the characteristic of capillary condensation of N_2 molecules in mesopores. The corresponding PSD data calculated from the desorption branch of the nitrogen isotherms by the BJH method revealed that the pores on the shell were mainly centered at ca. 2.3 nm, which matched well with the TEM data. Some larger pores of around 3.8 nm existed as well. The BET surface areas of the samples prepared with different $C_{16}TMABr/CaCO_3$ or the corresponding $C_{16}TMABr/SiO_2$ ratios via Method I were collected in Table 1. It showed that the MHSNTs prepared with a certain $C_{16}TMABr/SiO_2$ ratio (*B*) had the highest BET surface area. To further investigate the effects of the different templates removing methods, samples were prepared separately by Methods I–III with $C_{16}TMABr/SiO_2$ ratio *B* and the results were shown in Table 2. By Method II, the BET surface area could reach 975.3 m^2/g and the pore volume was ~0.916 cm^3/g with an average pore size of ~3 nm.

Table 1
The BET values of samples prepared at different ratios via Method I

Sample via Method I	*A*	*B*	*C*	*D*
$C_{16}TMABr/CaCO_3$ (molar ratio)	0.2 (1:5)	0.133 (1:7.5)	0.1 (1:10)	0
$C_{16}TMABr/SiO_2$ (molar ratio)	0.278	0.185	0.139	0
BET (m^2/g)	738.2	774.9	695.2	277.4

Table 2
The pore structural analysis of samples prepared at ratio *B* with Methods I–III

Sample *B*	Method I	Method II	Method III
BET (m^2/g)	774.9	975.3	895.6
Pore volume (cm^3/g)	0.696	0.916	0.742
Average pore size (nm)	3.52	3.04	2.47

Fig. 5 showed the small-angle XRD patterns of the MHSNTs. One intense diffraction peak at $2\theta = 2.4-2.5^\circ$, which is the characteristic of mesoporous materials with a worm-hole structure lacking long-range order [28], was observed for all samples except the one with $C_{16}TMABr/SiO_2$ ratio *D* (=0). Moreover, the intensity of the diffraction peak increased in the order *b* (ratio *B*) > *a* (ratio *A*) > *c* (ratio *C*) > *d* (ratio *D*). This result demonstrated that the mesopores on the hollow silica shell are introduced by $C_{16}TMABr$ and the amount of the added $C_{16}TMABr$ influences the structure of mesopores greatly.

The small-angle XRD patterns of the MHSNTs synthesized by different methods (Methods I–III), shown in Fig. 6, revealed that the intensity of the diffraction peak at $2\theta = 2.4-2.5^\circ$ of the sample prepared by Method II (curve a) was much higher than those via the other two methods, and that of Method III

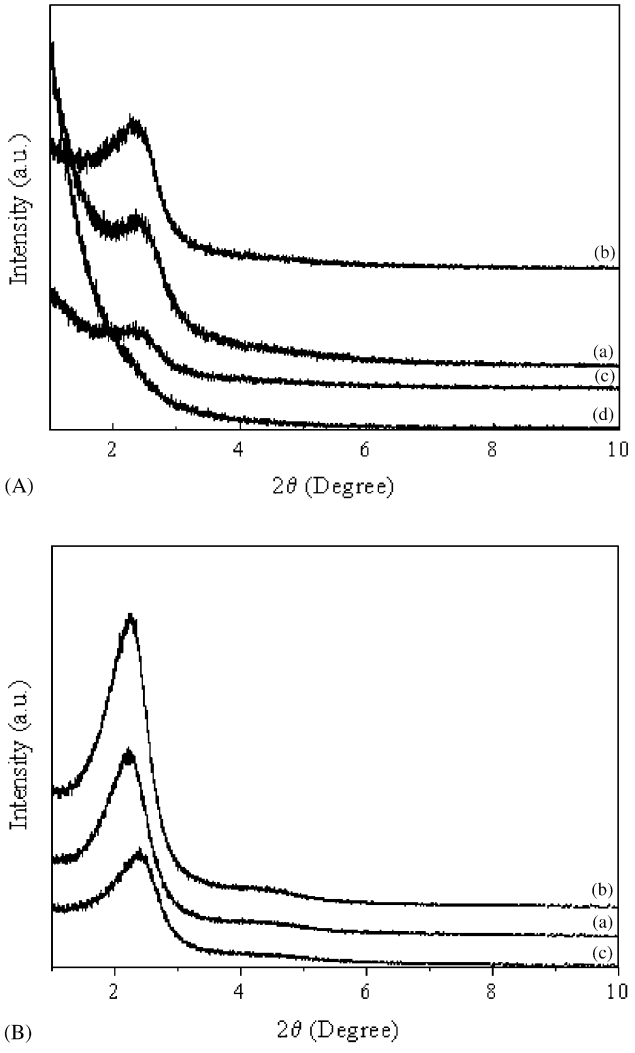

Fig. 5. The small-angle XRD patterns of MHSNTs prepared with different $C_{16}TMABr/SiO_2$ ratios by Methods I (A) and II (B): a—ratio *A*; b—ratio *B*; c—ratio *C*; d—ratio *D*.

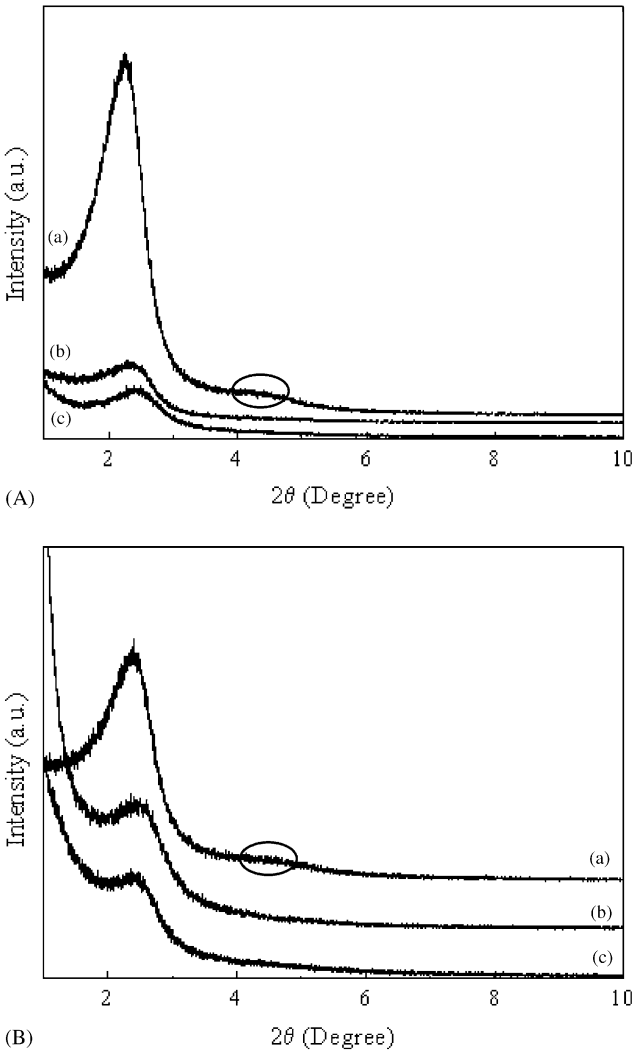

Fig. 6. The small-angle XRD patterns of MHSNTs prepared by different templates removing methods with $C_{16}TMABr/SiO_2$ ratio *B* (A) and ratio *A* (B): a—Method II; b—Method III; c—Method I.

(curve b) was a little stronger than that by Method I (curve c). In addition, there was another weak peak near $2\theta = 4.5^\circ$ in curve (a), which did not exist in curves (b) and (c). These results indicated that the ordered structure of the mesopores in MHSNTs could be better maintained after the extraction process (Method II) to remove the templates, which is in good agreement with the change of the corresponding BET and pore volumes shown in Table 2. Although the reason is unclear, it can be assumed that the solvent extraction may provide a more moderate condition to remove the surfactant template than the calcinating process, and therefore could effectively prevent the collapse of the pore structures and the coking of surfactants, which can easily occur during the calcinating process and demolish the order of the mesopores. In addition, the simultaneous removal of the double templates by a single process in Method II might cause less damage to the mesoporous channels than the separate two processes (calcination and etching in an acetic acid) in Method I. Since acetic acid owns a weaker acidity than HCl and can also act as an extracting agent for $C_{16}TMABr$, the use of acetic acid in Method II causes less disruption of the mesopores as compared to that resulting from the drastic reaction between $CaCO_3$ and HCl in Method III, leading to a more uniform mesoporous structure in Method II. This may also be the reason for the largest BET ($975.3\,m^2/g$) obtained in Method II.

The broad-angle XRD and FTIR were also employed to further study the formation process of MHSNTs under different conditions. Fig. 7 showed the XRD patterns of the needle-like $CaCO_3$ templates, the $CaCO_3/SiO_2$ composites before and after calcinations, and the as-prepared MHSNTs with different methods for the removal of templates. Curve (a) revealed a typical crystal structure of the needle-like $CaCO_3$

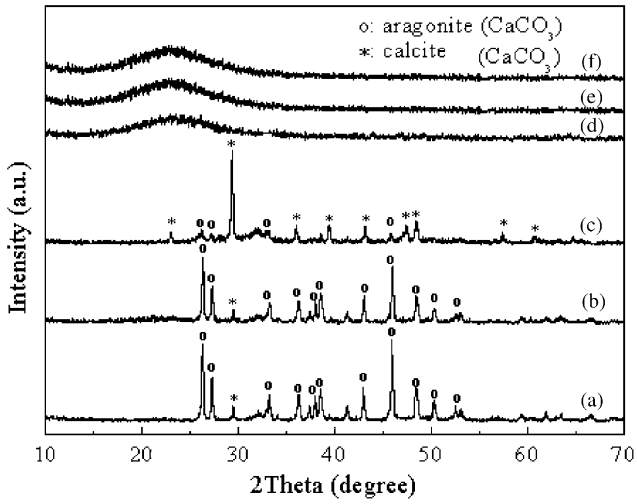

Fig. 7. XRD patterns of the needle-like $CaCO_3$ (a), $CaCO_3/SiO_2$ composites before (b) and after (c) calcination, and MHSNTs (d–f) by Methods I–III.

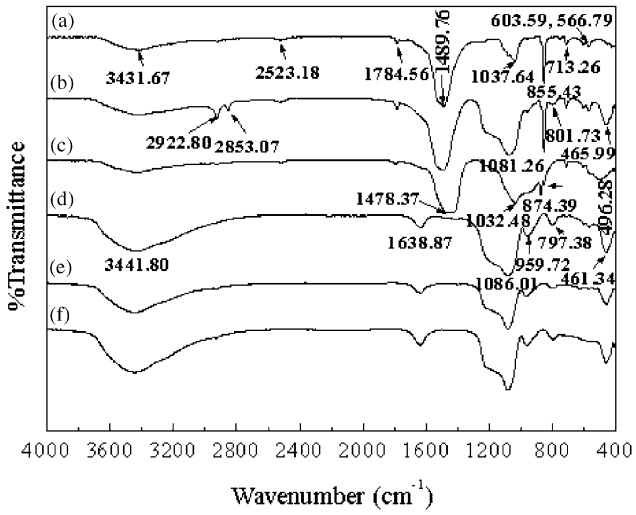

Fig. 8. FTIR patterns of the needle-like $CaCO_3$ (a), $CaCO_3/SiO_2$ composites before (b) and after (c) calcination, and MHSNTs (d–f) by Methods I–III.

template, which consisted mainly of aragonite phase with a little calcite content. Compared with curve (a), the intensity of the diffraction peaks of curve (b) for the pre-calcinated $CaCO_3/SiO_2$ composites decreased slightly due to the formation of the amorphous SiO_2 coating layer on the surface of $CaCO_3$. After being calcinated at 823 K, the content of calcite increased while that of aragonite decreased, which could be determined by the transformation of crystallographic forms and the change of the intensity of the diffraction peaks as shown in curve (c). The broad diffraction peaks at around 23°, which correspond to the amorphous silica structure, in curves (d–f) are exactly the same, indicating that the MHSNTs obtained through Methods I–III have the same structure. The XRD data could also verify that the inorganic and organic templates can be removed completely by the different methods in this work.

The FTIR study confirmed the results from the XRD analysis. Fig. 8 showed the IR spectra of the needle-like $CaCO_3$ templates (curve a), the $SiO_2/CaCO_3$ composites before (curve b) and after (curve c) calcination, and the MHSNTs (curves d–f) prepared by Methods I, II and III, respectively. The bands at 2922.8 and 2853.07 cm^{-1} for the surfactant C_{16}TMABr, and 1081.26, 801.73 and 465.99 cm^{-1} for the silica layer were shown in curve (b), along with the needle-like $CaCO_3$ bands in curve (a). After the thermal treatment at 823 K, the bands at 2922.8 and 2853.07 cm^{-1} disappeared due to the removal of C_{16}TMABr, while some other bands had a little shift probably owing to the transformation of $CaCO_3$ crystallographic form. After the template removing processes, only the major bands near 3441.8, 1638.87, 1086.01, 959.72, 797.38 and 461.34 cm^{-1} were left in curves (d–f), which are the IR spectroscopy of silica [29]. No C_{16}TMABr or $CaCO_3$ residue could be detected. The bands at 3441.8 and 1638.87 cm^{-1} are associated with the constitutional water, and those at 1086.01, 959.72, 797.38 and 461.34 cm^{-1} are attributed to the Si–OH stretching, Si–O–Si asymmetric stretching, symmetric stretching and bending vibrations, respectively.

4. Conclusion

MHSNTs have been successfully fabricated from the self-assembly of the surfactant and silica on the surface of needle-like calcium carbonate nanoparticles in an alkaline medium at room temperature. MHSNTs have a uniform tubular hollow structure with big openings, a length of 1.5–2.0 μm, an inner diameter of 150–200 nm at the open end and 50–60 nm at the closed end, and a wall thickness of 20–30 nm, a narrow PSD around 2.3 nm in the shells as well as a high BET surface area of ~975.3 m^2/g. Two methods to remove the double templates were employed. It was found that the simultaneous removal of the double templates during the extraction process would produce more uniformly structured mesopores on the shell than the separate removal processes of the double templates by calcinating and then etching in an acidic solution. This novel silica material with specific structures may be widely applied for catalysis, controlled drug release and immobilization of bio-macromolecules, such as proteins and enzymes.

Acknowledgments

The authors gratefully acknowledge the financial supports provided by National Natural Science Foun-

dation of China (No. 20325621, 20236020), National "973" program of China (No. 2003CB615807), the Program for New Century Excellent Talents in University (No. NCET-04-0123), National "863" Program of China (No. 2003AA302620), Beijing Municipal Commission of Education (JD100100403), CNPC Innovation Foundation, the Talent Training Program of Beijing City (H020821270120) and SRF for ROCS, SEM.

References

[1] Y. Xia, P. Yang, Y. Sun, Y. Wu, B. Mayer, B. Gates, Y. Yin, F. Kim, H. Yan, Adv. Mater. 15 (2003) 353.
[2] Z.L. Wang, Adv. Mater. 12 (2000) 1295.
[3] J. Jang, B.K. Lim, J. Lee, T. Hyeon, Chem. Commun. (2001) 83.
[4] K.J.C. van Brommel, A. Friggeri, S. Shinkai, Angew. Chem. Int. Ed. 42 (2003) 980.
[5] H. Nishikawa, T. Shiroyama, R. Nakamura, Y. Ohki, Phys. Rev. B 45 (1992) 586.
[6] J. Jang, B. Lim, Adv. Mater. 14 (2002) 1390.
[7] D.T. Mitchell, S.B. Lee, L. Trofin, N. Li, T.K. Nevanen, H. Soderlund, C.R. Martin, J. Am. Chem. Soc. 124 (2002) 11864.
[8] Y. Zhang, K. Suenaga, C. Colloex, S. Lijima, Science 281 (1998) 973.
[9] J.Q. Hu, Y. Bando, K. Wada, L.L. Cheng, P. Pirouz, Appl. Phys. Lett. 80 (2002) 491.
[10] S. Baral, P. Schoen, Chem. Mater. 5 (1993) 145.
[11] W. Shenton, T. Douglas, M. Young, G. Stubbs, S. Mann, Adv. Mater. 11 (1999) 253.
[12] F. Miyaji, S.A. Davis, J.P.H. Charmant, S. Mann, Chem. Mater. 11 (1999) 3021.
[13] J.H. Jung, S. Shinkai, T. Shimizu, Nano Lett. 2 (2002) 17.
[14] M. Harada, M. Adachi, Adv. Mater. 12 (2002) 839.
[15] M. Adachi, T. Harada, M. Harada, Langmuir 16 (2000) 2376.
[16] B.C. Satishkumar, A. Govindaraj, E.M. Vogl, L. Basumallick, C.N.R. Rao, J. Mater. Res. 12 (1997) 604.
[17] R. Fan, Y.Y. Wu, D.Y. Li, M. Yue, A. Majumdar, P.D. Yang, J. Am. Chem. Soc. 125 (2003) 5254.
[18] S.O. Obare, N.R. Jana, C.J. Murphy, Nano Lett. 1 (2001) 601.
[19] B.B. Lakshmi, C.J. Patrissi, C.R. Martin, Chem. Mater. 9 (1997) 2544.
[20] J. Jang, H. Yoon, Adv. Mater. 19 (2004) 799.
[21] C. Hippe, M. Wark, E. Lork, G. Schulz-Ekloff, Micro. Meso. Mater. 31 (1999) 235.
[22] Y. Le, J.F. Chen, J.X. Wang, L. Shao, W.C. Wang, Mater. Lett. 58 (2004) 2105.
[23] J.F. Chen, J.X. Wang, R.J. Liu, L. Shao, L.X. Wen, Inorg. Chem. Commun. 7 (2004) 447.
[24] J.X. Wang, L.X. Wen, Z.H. Wang, M. Wang, L. Shao, J.F. Chen, Scr. Mater. 51 (2004) 1035.
[25] M. Wang, H.K. Zou, L. Shao, J.F. Chen, Powder Technol. 142 (2004) 166.
[26] G.S. Zhu, S.L. Qiu, O. Terasaki, Y. Wei, J. Am. Chem. Soc. 123 (2001) 7723.
[27] P.V. Braun, S.I. Stupp, Mater. Res. Bull. 34 (1999) 463.
[28] S.A. Bagshaw, E. Prouzet, T.J. Pinnavaia, Science 269 (1995) 1242.
[29] J.R. Martinez, F. Ruiz, Y.V. Vorobiev, J. Chem. Phys. 109 (1998) 7511.